Inorganic Chemistry
Article

Inorg. Chem. **2009**, *48*, 10581–10590 **10581**
DOI: 10.1021/ic901112s

Dioxomolybdenum(VI) Complexes with Ene-1,2-dithiolate Ligands: Synthesis, Spectroscopy, and Oxygen Atom Transfer Reactivity

Hideki Sugimoto,*,† Susumu Tatemoto,† Koichiro Suyama,‡ Hiroyuki Miyake,‡ Shinobu Itoh,*,† Chao Dong,§ Jing Yang,§ and Martin L. Kirk*,§

†*Department of Material and Life Science, Graduate School of Engineering, Osaka University, 2-1 Yamada-oka, Suita, Osaka 565-0871, Japan,* ‡*Department of Chemistry, Graduate School of Science, Osaka City University, 3-3-138 Sumiyoshi-ku, Osaka 558-8585, Japan, and* §*Department of Chemistry and Chemical Biology, The University of New Mexico, MSC03 2060, 1 University of New Mexico, Albuquerque, New Mexico 87131-0001*

Received June 9, 2009

New dioxomolybdenum(VI) complexes, $(Et_4N)(Ph_4P)[Mo^{VI}O_2(S_2C_2(CO_2Me)_2)(bdt)]$ (**2**) and $(Et_4N)(Ph_4P)[Mo^{VI}O_2(S_2C_2(CO_2Me)_2)(bdtCl_2)]$(**4**)($S_2C_2(CO_2Me)_2$ = 1,2-dicarbomethoxyethylene-1,2-ditholate, bdt = 1,2−benzenedithiolate, $bdtCl_2$ = 3,6-dichloro-1,2-benzenedithiolate), that possess at least one ene-1,2-dithiolate ligand were synthesized by the reaction of their mono-oxo-molybdenum(IV) derivatives, $(Et_4N)_2[Mo^{IV}O(S_2C_2(CO_2Me)_2)(bdt)]$ (**1**) and $(Et_4N)_2[Mo^{IV}O(S_2C_2(CO_2Me)_2)(bdtCl_2)]$ (**3**), with Me_3NO. Additionally, the bis(ene-1,2-dithiolate)$Mo^{VI}O_2$ complex, $(Et_4N)(Ph_4P)[Mo^{VI}O_2(S_2C_2(CO_2Me)_2)_2]$ (**6**), was isolated. Complexes **2**, **4**, and **6** were characterized by elemental analysis, negative-ion ESI mass spectrometry, and IR spectroscopy. X-ray analysis of **4** and **6** revealed a Mo^{VI} center that adopts a distorted octahedral geometry. Variable-temperature ^{1}H NMR spectra of $(CD_3)_2CO$ solutions of the $Mo^{VI}O_2$ complexes indicated that the Mo centers isomerize between Δ and Λ forms. The electronic structures of **2**, **4**, and **6** have been investigated by electronic absorption and resonance Raman spectroscopy and bonding calculations. The results indicate very similar electronic structures for the complexes and considerable π-delocalization between the $Mo^{VI}O_2$ and ene-1,2-dithiolate units. The similar oxygen atom transfer kinetics for the complexes results from their similar electronic structures.

Introduction

The periplasmic DMSO reductases (DMSOR)[1,2] are pyranopterin molybdenum enzymes that contain the Mo active site as their only redox-active center and function as terminal electron acceptors during anaerobic growth of *R. sphaeroides* and *R. capsulatus* in the presence of DMSO. Consensus structures for the oxidized and reduced DMSOR family members are shown in Figure 1.[3] The absence of additional chromophores in DMSOR has allowed for their characterization by resonance Raman (rR),[4] electronic absorption[5] and, for a glycerol inhibited form, magnetic circular dichroism (MCD) spectroscopy.[6] The absorption spectra for the Mo^{VI} and Mo^{IV} forms of *R. sphaeroides* and *R. capsulatus* DMSOR display low energy absorption bands at 720 ($\sim$2000 M^{-1} cm^{-1}) and 640 nm ($\sim$1000 M^{-1} cm^{-1}) respectively, and their intensity implies significant charge transfer character.[5] Additionally, rR spectroscopy[7] provides evidence for vibrational modes that are sensitive to ^{34}S isotopic substitution. These data provide strong evidence that the observed low energy optical transitions possess considerable S(ene-1,2-dithiolate) → Mo charge transfer (CT) character.

It is therefore of interest to understand how bis(ene-1,2-dithiolate) coordination in members of the DMSOR family of enzymes affects electron and atom transfer reactivity during the course of catalysis. This interest arises from the fact that ene-1,2-dithiolates and dithiolenes are highly noninnocent ligands that have a dramatic effect on the electronic structure of their metal ion complexes.[8] It has been suggested that the

*To whom correspondence should be addressed. E-mail: sugimoto@mls.eng.osaka-u.ac.jp (H.S.); shinobu@mls.eng.osaka-u.ac.jp (S.I.); mkirk@unm.edu (M.L.K.).

(1) Hille, R. *Chem. Rev.* **1996**, *96*, 2757–2816.
(2) Hille, R. *Molybdenum Enzymes Containing the Pyranopterin Cofactor: An Overview*; Marcel Dekker, Inc.: New York, 2002; Vol. *39*, p 187−226.
(3) Li, H.-K.; Temple, C.; Rajagopalan, K. V.; Schindelin, H. *J. Am. Chem. Soc.* **2000**, *122*, 7673–7680.
(4) Garton, S. D.; Temple, C. A.; Dhawan, I. K.; Barber, M. J.; Rajagopalan, K. V.; Johnson, M. K. *J. Biol. Chem.* **2000**, *275*, 6798–6805.
(5) Cobb, N.; Conrads, T.; Hille, R. *J. Biol. Chem.* **2005**, *280*, 11007–11100.
(6) Finnegan, M. G.; Hilton, J.; Rajagopalan, K. V.; Johnson, M. K. *Inorg. Chem.* **1993**, *32*, 2616–2617.
(7) Johnson, M. K. *Prog. Inorg. Chem.* **2004**, *52*, 213–266.
(8) Kirk, M. L.; Helton, M. E.; McNaughton, R. L. *Prog. Inorg. Chem.* **2004**, *52*, 111–212.

Published on Web 10/15/2009

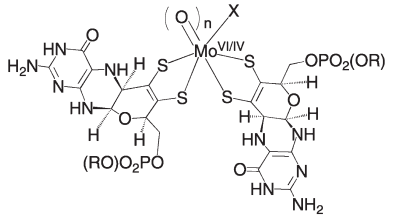

Figure 1. Structure of oxidized ($n = 1$) and reduced ($n = 0$) molybdenum centers in the DMSOR family.

degree of π-delocalization within the dithiolene unit and charge donation to the metal can be monitored by the frequency of the ν(C=C) stretching mode associated with the ene−1,2−dithiolate ligand (−S−C=C−S−).[7] However, in some enzymes of the DMSOR family, the ν(C=C) stretch is often difficult to observe or definitively assign by rR spectroscopy because of the intense absorption features of additional prosthetic groups, such as flavins, Fe−S clusters, or hemes. Even in the absence of these chromophores, it can be difficult to unambiguously assign the ν(C=C) stretch without an isotope perturbation. However, the ν(C=C) stretch has been assigned in a number of DMSOR family enzymes using rR spectroscopy.[7] In these studies, the ν(C=C) stretch has been shown to range from 1525 to 1598 cm^{-1} in arsenite oxidase (AO)[9] and from 1526 to 1576 cm^{-1} for DMSOR[10] during their respective reaction catalytic cycles.

The information gleaned from the ν(C=C) stretching frequency, coupled with an understanding of the electronic origins of the CT spectra in DMSOR family enzymes, can provide deeper insight into electronic structure contributions to the rich electron and atom transfer reactivity of DMSOR family enzymes. Structurally characterized model compounds can serve as important benchmarks for evaluating enzyme spectra and developing key structure−function relationships. Along these lines, more than two dozen $[Mo^{IV}O(ene\text{-}1,2\text{-}dithiolate)]^{2-}$ complexes have been synthesized as analogues of reduced DMSOR family enzymes and characterized by IR and rR spectroscopies.[11−13] Recently, we reported a $Mo^{IV}O$ complex which possesses both an ene-1,2-dithiolate ligand and an aromatic dithiolene ligand, $(Et_4N)_2[Mo^{IV}O(S_2C_2(CO_2Me)_2)(bdt)]$ (**1**) (Chart 1, $S_2C_2(CO_2Me)_2$ = 1,2-dicarbomethoxyethylene-1,2-ditholate, bdt = 1,2-benzenedithiolate).[14] In contrast, Mo^{VI} complexes with one or two ene-1,2-dithiolate ligands have been considered to be unstable for isolation as a result of autoredox reactions that may be facilitated by π-delocalization between the metal and ene-1,2-dithiolate ligands.[12,15−18] Isolated Mo^{VI} $[Mo^{VI}O_2(ene\text{-}1,2\text{-}dithiolate)_2]^{2-}$ complexes are limited to $[MoO_2(mnt)_2]^{2-}$ (mnt = dicyanoethylene-1,2-dithiolate),[19] which is believed to be stabilized by the very strong electron withdrawing nature of the CN substituents. Other $Mo^{VI}O_2$ or $Mo^{VI}O(OR)$ bis(ene-1,2-dithiolate) complexes have been generated in situ.[15−18] Thus, there is a need for spectroscopic and electronic structure studies on structurally characterized model systems that do not have substituents in conjugation with the C=C unit of the ene-1,2-dithiolate ligand, since the pyranopterin cofactor is not believed to be conjugated to the ene-1,2-dithiolate moiety in the enzymes.[1,20]

Chart 1. Designation and Abbreviation of Complex Structures

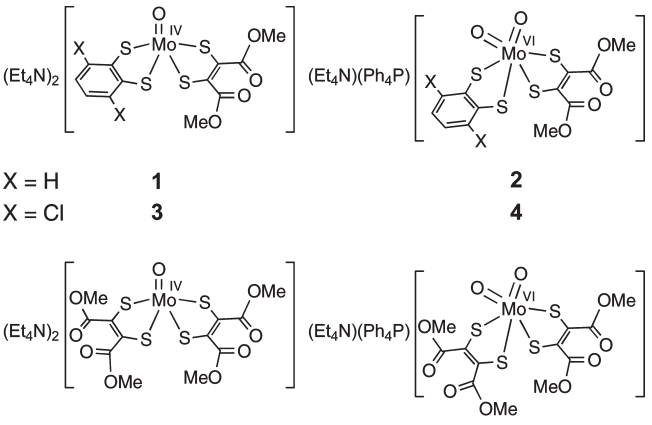

In this manuscript, we describe the synthesis of $(Et_4N)(Ph_4P)[Mo^{VI}O_2(S_2C_2(CO_2Me)_2)(bdt)]$ (**2**) and its chlorine substituted aromatic dithiolene derivative, $(Et_4N)(Ph_4P)$-$[Mo^{VI}O_2(S_2C_2(CO_2Me)_2)(bdtCl_2)]$ (**4**). Additionally, the X-ray structure of **4** has been determined. These $Mo^{VI}O_2$ complexes possess one ene-1,2-dithiolate ligand in addition to an aromatic dithiolene ligand (Chart 1). A particular advantage of this mixed dithiolene ligand set is the ability to isolate stable d^0 dioxo $Mo^{VI}O_2$ complexes as well as their d^2 monooxo $Mo^{IV}O$ counterparts.[21−27] We were also able to isolate and characterize the dioxo complex $(Et_4N)(Ph_4P)[Mo^{VI}O_2(S_2C_2(CO_2Me)_2)_2]$ (**6**), which had previously been considered too unstable for isolation.[12] Finally, we have used electronic absorption and resonance Raman spectroscopies to probe the basic electronic structure of the dioxo complexes, and this has provided insight into the relationship between their electronic structure properties and oxygen atom transfer reactivity.

Experimental Section

General. All reagents and solvents were used as received unless otherwise noted. All reactions were carried out under a

(9) Conrads, T.; Hemann, C.; George, G. N.; Pickering, I. J.; Prince, R. C.; Hille, R. *J. Am. Chem. Soc.* **2002**, *124*, 11276–11277.
(10) Garton, S. D.; Hilton, J.; Oku, H.; Crouse, B. R.; Rajagopalan, K. V.; Johnson, M. K. *J. Am. Chem. Soc.* **1997**, *119*, 12906–12916.
(11) Sugimoto, H.; Tsukube, H. *Chem. Soc. Rev.* **2008**, *37*, 2609–2619.
(12) Enemark, J. H.; Cooney, J. J. A.; Wang, J.-J.; Holm, R. H. *Chem. Rev.* **2004**, *104*, 1175–1200.
(13) McMaster, J.; Tunney, J. M.; Garner, C. D., *Chemical Analogues of the Catalytic Centers of Molybdenum and Tungsten Dithiolene-Containing Enzymes*; John Wiley and Sons, Inc: Hoboken, NJ, 2004; Vol. *52*, p 539−584.
(14) Sugimoto, H.; Suyama, K.; Sugimoto, K.; Miyake, H.; Takahashi, I.; Hirota, S.; Itoh, S. *Inorg. Chem.* **2008**, *47*, 10150–10157.
(15) Sugimoto, H.; Harihara, M.; Shiro, M.; Sugimoto, K.; Tanaka, K.; Miyake, H.; Tsukube, H. *Inorg. Chem.* **2005**, *44*, 6386–6392.
(16) Lim, B. S.; Holm, R. H. *J. Am. Chem. Soc.* **2001**, *123*, 1920–1930.
(17) Oku, H.; Ueyama, N.; Nakamura, A. *Inorg. Chem.* **1997**, *36*, 1504–1516.
(18) Oku, H.; Ueyama, N.; Nakamura, A. *Inorg. Chem.* **1995**, *34*, 3667–3676.
(19) Das, S. K.; Chaudhury, P.; Biswas, D.; Sarkar, S. *J. Am. Chem. Soc.* **1994**, *116*, 9061–9070.
(20) Burgmayer, S. J. N. *Dithiolenes in Biology*; John Wiley and Sons, Inc.: Hoboken, NJ, 2004; Vol. *52*, p 491−538.
(21) Wang, J. J.; Holm, R. H. *Inorg. Chem.* **2007**, *46*, 11156–11164.
(22) Sugimoto, H.; Tarumizu, M.; Miyake, H.; Tsukube, H. *Eur. J. Inorg. Chem.* **2006**, 4494–4497.
(23) Sugimoto, H.; Tarumizu, M.; Tanaka, K.; Miyake, H.; Tsukube, H. *Dalton Trans.* **2005**, 3558–3565.
(24) Partyka, D. V.; Holm, R. H. *Inorg. Chem.* **2004**, *43*, 8609–8616.
(25) Lim, B. S.; Willer, M. W.; Miao, M. M.; Holm, R. H. *J. Am. Chem. Soc.* **2001**, *123*, 8343–8349.
(26) Donahue, J. P.; Goldsmith, C. R.; Nadiminti, U.; Holm, R. H. *J. Am. Chem. Soc.* **1998**, *120*, 12869–12881.
(27) Ueyama, N.; Oku, H.; Kondo, M.; Okamura, T.-a.; Yoshinaga, N.; Nakamura, A. *Inorg. Chem.* **1996**, *35*, 643–650.

dinitrogen atmosphere using standard Schlenk techniques. $(Et_4N)_2[Mo^{IV}O(S_4)(bdtCl_2)]$, $(Et_4N)_2[Mo^{IV}O(S_2C_2(CO_2Me)_2)(bdt)]$ (**1**), and $(Et_4N)_2[Mo^{IV}O(S_2C_2(CO_2Me)_2)_2]$ (**5**) were prepared by following established literature procedures.[14,28]

Synthesis and Characterization of Complexes. $(Et_4N)(Ph_4P)[Mo^{VI}O_2(S_2C_2(CO_2Me)_2)(bdt)]$ (2). An acetonitrile solution of 1 mL containing Me_3NO (trimethylamine *N*-oxide, 4.8 mg, 0.064 mmol) was added to 3 mL of an acetonitrile solution containing **1** (23.2 mg, 0.032 mmol) and Ph_4PBr (41.2 mg, 0.098 mmol). The resultant deep-red solution was concentrated to ~1 mL. The addition of 25 mL of ethanol to the solution gave a red−black microcrystalline powder of **2**, which was collected by filtration and dried in vacuo. Yield: 22.9 mg (73%). Anal. Calcd for $C_{44}H_{50}MoO_6NPS_4 \cdot 3H_2O$ (mol wt 999.09): C, 52.95; H, 5.66; N, 1.40. Found: C, 53.33; H, 5.27; N; 1.62. ^{1}H NMR (CD_3CN, 25 °C, anionic part): δ 7.03 (m, 2H), 6.58 (m, 2H), 3.58 (s, 6H). UV−vis spectrum (CH_3CN): λ_{max} = 362 (ε = 8130), 422 (sh, 4970), 530 nm (1880 M^{-1} cm^{-1}). ESI−MS (CH_3CN): m/z = 606 $\{[M]^{2-} + Et_4N^+\}^-$, 815 $\{[M]^{2-} + Ph_4P^+\}^-$. CV (CH_3CN): E_{pc} (irrev.) = −1.70 V vs SCE. IR (KBr): ν 528 (vs), 691 (s), 723 (s), 759 (m), 836 (s), 870 (s), 997 (m), 1026 (s), 1077 (w), 1108 (vs), 1236 (vs), 1438 (vs), 1484 (s), 1586 (w), 1707 (s), 1716 cm^{-1} (s).

$(Et_4N)_2[Mo^{IV}O(S_2C_2(CO_2Me)_2)(bdtCl_2)]$ (3). This complex was synthesized using the same procedure as **1**,[14] except $(Et_4N)_2[MoO(S_4)(bdtCl_2)]$ (224 mg, 0.316 mmol) was used instead of $(Et_4N)_2[MoO(S_4)(bdt)]$. Yield: 166 mg (67%). Anal. Calcd for $C_{28}H_{48}Cl_2MoN_2O_5S_4$ (mol wt 787.81): C, 42.69; H, 6.14; N, 3.56. Found: C, 42.83; H, 6.09; N; 3.53. ^{1}H NMR (CD_3CN, anionic part): δ 6.89 (s, 2H), 3.70 (s, 6H). UV−vis spectrum (CH_3CN): λ_{max} = 377 (ε = 3490), 431 (870), 531 nm (340 M^{-1} cm^{-1}). ESI−MS (CH_3CN): m/z = 264 $[M]^{2-}$, 658 $\{[M]^{2-} + Et_4N^+\}^-$. CV (CH_3CN): $E_{1/2}$(rev.) = −0.11 V vs SCE. IR (KBr): ν 784 (m), 807 (m), 909 (s), 999 (m), 1017 (m), 1055 (m), 1152 (m), 1172 (m), 1234 (vs), 1325 (m), 1394 (s), 1431 (m), 1454 (m), 1483 (s), 1528 (s), 1696 (s), 1711 cm^{-1} (s).

$(Et_4N)(Ph_4P)[Mo^{VI}O_2(S_2C_2(CO_2Me)_2)(bdtCl_2)]$ (4). To 10 mL of an acetonitrile solution of **3** (50.9 mg, 0.065 mmol), 4 mL of an acetonitrile solution of Me_3NO (10.0 mg, 0.133 mmol) was added. The resultant deep−red solution was stirred for 5 min, and then Ph_4PBr (87.0 mg, 0.207 mmol) was added to the solution. A brown powder was precipitated by addition of ethanol to the solution, and this was collected by filtration and dried in vacuo. Yield: 50.5 mg (75%). Anal. Calcd for $C_{44}H_{48}MoNO_6PS_4 \cdot H_2O$ (mol wt. 1030.95): C, 51.26; H, 4.89; N, 1.36. Found: C, 51.13; H, 4.76; N; 1.55. ^{1}H NMR (CD_3CN, 25 °C, anionic part): δ 6.73 (s, 2H), 3.59 (s, 6H). UV−vis spectrum (CH_3CN): λ_{max} = 329 (ε = 6670), 358 (5040), 417 (3000), 525 nm (1100 M^{-1} cm^{-1}). ESI−MS (CH_3CN): m/z = 674 $\{[M]^{2-} + Et_4N^+\}^-$, 883 $\{[M]^{2-} + Ph_4P^+\}^-$. CV (CH_3CN): E_{pc}(irrev.) = −1.66 V vs SCE. IR (KBr): ν 528 (vs), 691 (s), 723 (s), 757 (m), 838 (s), 872 (s), 997 (m), 1027 (s), 1068 (s), 1109 (vs), 1154 (m), 1236 (vs), 1333 (m), 1394 (vs), 1437 (vs), 1483 (vs), 1585 (w), 1680 (s), 1715 cm^{-1} (s).

$(Et_4N)(Ph_4P)[Mo^{VI}O_2(S_2C_2(CO_2Me)_2)_2]$ (6). An acetonitrile solution (1 mL) containing Me_3NO (6.6 mg, 0.084 mmol) was added to an acetonitrile solution (5 mL) containing **5** (31.3 mg, 0.040 mmol). An acetonitrile solution (2 mL) of Ph_4PBr (50.2 mg, 0.120 mmol) was immediately added to the reaction mixture and the resultant deep−red solution was concentrated to ca. 1 mL. When a solution composed of 6 mL of ethanol and 10 mL of diethyl ether was added to the deep-red solution, a red−black microcrystalline powder (**6**) precipitated from the solution. This was collected by filtration and dried in vacuo. Yield: 28.2 mg (70%). Anal. Calcd for $C_{44}H_{52}MoNO_{10}PS_4$ (mol wt. 1010.75): C, 52.32; H, 5.19; N, 1.39. Found: C, 52.35; H, 4.99; N; 1.52. ^{1}H NMR (CD_3CN, 25 °C, anionic part): δ 3.60 (s, 12H). UV−vis spectrum (CH_3CN): λ_{max} = 358 (ε = 7630), 419 (5370), 536 nm (1840 M^{-1} cm^{-1}). ESI−MS (CH_3CN): m/z = 542 $[M]^-$, 672 $\{[M]^{2-} + Et_4N^+\}^-$, 881 $\{[M]^{2-} + Ph_4P^+\}^-$. CV (CH_3CN): E_{pc} (irrev.) = −1.70 V vs SCE. IR (KBr): ν 528 (vs), 692 (s), 724 (s), 763 (m), 838 (s), 869 (s), 997 (m), 1026 (s), 1076 (w), 1109 (vs), 1233 (vs), 1436 (vs), 1484 (s), 1685 (vs), 1708 cm^{-1} (vs).

Physical Measurements. ^{1}H NMR spectra were recorded with a JEOL Lambda 300, and the TMS signal was adjusted to 0 ppm. ESI−MS spectra were measured with a JEOL JMS−700S. FT−IR spectra were recorded with a Perkin-Elmer Spectrum One spectrometer. Routine UV−vis spectra were recorded on a Shimazu−UV 2550 spectrometer. Additional solution electronic absorption spectra were collected using a Hitachi U-3501 UV−Vis−NIR dual-beam spectrometer capable of scanning a wavelength region between 185 and 3200 nm. Spectral samples were dissolved in dry, degassed dichloromethane, and the electronic absorption spectra were measured in a 1-cm path length, 100 μL, black-masked, quartz cuvette (Starna Cells, Inc.) equipped with a Teflon stopper. All electronic absorption spectra were performed at room temperature and repeated at regular time intervals to ensure the structural stability and integrity of the complex in solution. Solid-state resonance Raman (rR) spectra and associated rR excitation profiles were collected using a system comprised of an PI/Acton SpectraPro SP-2500i 500 mm focal length imaging spectrograph with a triple grating turret and a PI/Acton Spec-10:100B back-illuminated 1340 × 100 pixel digital CCD spectroscopy system with a cryogenically cooled camera head. A Coherent Innova I302C Ar^+ ion laser was the excitation source. Samples were mixed with either NaCl or a $NaCl/Na_2SO_4$ mixture with Na_2SO_4 as an internal calibrant.

Electrochemistry. Cyclic voltammetric measurements were performed under dinitrogen with a Hokuto Denko HZ-3000 potentiostat. A set of glassy-carbon working electrodes (circular, 3 mm diameter), a SCE reference electrode, and a platinum counter electrode were employed in these experiments.

X-ray Crystallography. Single crystals of $(Et_4N)(Ph_4P)[Mo^{IV}O(S_2C_2(CO_2Me)_2)(bdt)]$ (**1a**) were obtained from an acetonitrile solution of **1** in the presence of Ph_4PBr. Single crystals of **4** and **6** were obtained by diffusion of diethyl ether into each acetonitrile solution. Single crystals of $(Et_4N)_2[MoO_2(S_2C_2(CO_2Me)_2)_2]$ (**7**) were obtained by diffusion of diethyl ether into an acetonitrile solution containing **5** and Me_3NO. Each single crystal obtained was mounted on a glass fiber, and all X-ray data were collected at −173 °C on a Rigaku CCD diffractometer with monochromatic Mo Kα radiation. The structures were solved by direct methods[29] and expanded using DIRDIF 99.[30] The non−hydrogen atoms were refined anisotropically by full-matrix least-squares on F^2. The hydrogen atoms were attached at idealized positions on carbon atoms and were not refined. All structures in the final stages of refinement showed no movement in the atom positions. The calculations were performed using Single-Crystal Structure Analysis Software, version 3.8.[31] Crystallographic parameters are summarized in Table 1.

Electronic Structure Calculations. Spin-restricted gas phase geometry optimizations and vibrational frequency calculations for compounds **2**, **4**, and **6** were performed at the density functional level of theory using the Gaussian 03W software package.[32] All calculations employed the B3LYP hybrid functional. A LANL2DZ basis set with an effective core potential was used for Mo and a 6-31G* basis set was used for all light atoms. Input files were prepared using the molecule builder function in the Gaussview software package. Frontier molecular orbitals were generated for the optimized ground states of **2**, **4**, and **6**, and the contributions of each MO were further analyzed using the program AOMix.[33] Time-dependent DFT calculations were performed on the optimized ground state geometries, and the first 40 excited states were calculated. Electron density

(28) Coucouvanis, D.; Hadjikyriacou, A.; Toupadakis, A.; Koo, S. M.; Ileperuma, O.; Draganjac, M.; Salifoglou, A. *Inorg. Chem.* **1991**, *30*, 754–767.

Table 1. Crystallographic Data for **1a**, **4**, **6**, and **7**

	1a	4	6	7
formula	$C_{44}H_{50}MoNO_5PS_4$	$C_{44}H_{48}MoNO_6PS_4Cl_2$	$C_{88}H_{104}Mo_2N_2O_{20}P_2S_8$	$C_{28}H_{52}MoN_2O_{10}S_4$
fw	928.04	1012.93	2020.10	800.91
cryst syst	monoclinic	monoclinic	monoclinic	monoclinic
space group	$P2_1/c$	$P2_1/c$	Pc	$P2_1/c$
a, Å	12.769(3)	18.557(4)	17.610(2)	16.367(7)
b, Å	19.816(4)	12.900(2)	13.596(1)	10.809(4)
c, Å	17.395(3)	19.479(5)	19.795(2)	21.510(9)
β, deg	94.392(3)	104.704(5)	103.658(3)	108.404(6)
V, Å^3	4388.4(15)	4510.4(17)	4605.3(8)	3611(3)
Z	4	4	2	4
ρ, g cm^{-3}	1.405	1.492	1.457	1.473
μ, mm^{-1}	0.570	0.677	0.557	0.647
data	35262	44183	44597	32195
unique data	9950	9731	18153	10007
R1[a]	0.0450	0.0897	0.0470	0.0715
wR2 (F^2)[b]	0.1318	0.1598	0.1265	0.2373
GOF	1.000	0.868	0.975	1.081

[a] $R1 = \Sigma(|F_o| - |F_c|)/\Sigma|F_o|$. [b] $wR2 = \{\Sigma(w(F_o^2 - F_c^2)^2)/\Sigma w(F_o^2)^2\}^{1/2}$.

difference maps (EDDMs) were constructed using the Gauss-Sum suite of programs.[34]

Kinetic Measurements. For the oxygen atom transfer reactivity studies, CH_3CN:H_2O (3:2) solutions of the $Mo^{VI}O_2$ complexes and $NaAsO_2$ were prepared under dinitrogen. The progress of the atom transfer reactions from $Mo^{VI}O_2$ species to $NaAsO_2$ were performed at 20 °C, and the reaction progress was monitored spectroscopically using an HP 5453 diode array spectrometer. Each reaction was initiated by the injection of a CH_3CN:H_2O solution of $NaAsO_2$ through the septum cap of the quartz cell using a gastight syringe. The reactions were performed under pseudo first-order conditions with 10−70 equiv excess of $NaAsO_2$ over $[MoO_2]_0$ (1.5×10^{-4} M).

Results and Discussion

Preparation and Characterization of $Mo^{IV}O/Mo^{VI}O_2$ Complexes with $S_2C_2(CO_2Me)_2$. The complex $(Et_4N)_2$-$[Mo^{IV}O(S_2C_2(CO_2Me)_2)(bdtCl_2)]$ (**3**) ($S_2C_2(CO_2Me)_2$ = 1,2-dicarbomethoxyethylene-1,2-ditholate) was synthesized by a method previously used for the synthesis of $(Et_4N)_2$-$[Mo^{IV}O(S_2C_2(CO_2Me)_2)(bdt)]$ (**1**).[14] Complex **3** was then used as a precursor for the synthesis of the corresponding $Mo^{VI}O_2$ complex, **4**. The IR, ^{1}H NMR, and negative-ion ESI mass spectra of **3** were indicative of a mono-oxo $Mo^{IV}O$ center coordinated with one $S_2C_2(CO_2Me)_2^{2-}$ and one $bdtCl_2^{2-}$ ligand. Compound **3** exhibits a reversible redox wave for the Mo^V/Mo^{IV} redox process at −0.11 V vs SCE in acetonitrile. The potential is shifted by +0.13 V relative to **1** (−0.24 V) and this is an indication of a weaker $bdtCl_2^{2-}$ S→Mo charge donation when compared with the bdt^{2-} ligand.

The mono-oxo Mo(IV) compounds **1** and **3** were treated with Me_3NO to yield the corresponding isolable $Mo^{VI}O_2$ complexes via oxygen atom transfer. Upon addition of Me_3NO to an acetonitrile solution of **1** or **3**, the color was observed to change from orange to deep red. Deep red microcrystalline powders of $(Et_4N)(Ph_4P)$-$[Mo^{VI}O_2(S_2C_2(CO_2Me)_2)(L)]$ (**2**, L = bdt^{2-}; **4**, L = $bdtCl_2^{2-}$) were precipitated from the resulting solutions by addition of a slight excess of Ph_4PBr. The elemental analysis and negative-ion ESI−MS data (Figures S1 and S2, Supporting Information) for these deep red powders were consistent with the corresponding molecular formulas for these complexes. We note that compounds **2** and **4** are the first $Mo^{VI}O_2$ complexes to be synthesized that possess two different dithiolene ligands. Compound **6** was generated in acetonitrile from its precursor **5**, Me_3NO, and Ph_4PBr to yield a deep-red solution. A quick workup of this solution yielded a brown microcrystalline powder. The synthesis of **6** is important, since $[Mo^{VI}O_2(S_2C_2(CO_2Me)_2)_2]^{2-}$ had been assumed to be unstable with respect to oxidation due to an autoredox reaction between the Mo^{VI} ion and $S_2C_2(CO_2Me)_2^{2-}$ ligands.[12,18] Compound **6** was characterized in a manner similar to that of **2** and **4**, and its negative ESI−mass spectrum is given in Figure S3, Supporting Information. The three $Mo^{VI}O_2$ complexes, **2**, **4**, and **6**, exhibit temperature dependent ^{1}H NMR spectra. The temperature dependent spectrum for **4** is shown in Figure 2 as representative of the spectra for **2** and **6**. The ^{1}H NMR spectrum of **4** in $(CD_3)_2CO$ displays two singlets at δ = 6.73 and 3.59 ppm,

(29) Burla, M. C.; Camalli, M.; Carrozzini, B.; Cascarano, G. L.; Giacovazzo, C.; Polidori, G.; Spagna, R. *J. Appl. Crystallogr.* **2003**, *36*, 1103–1103.

(30) Beurskens, P. T.; Admiraal, G.; Beurskens, G.; Bosman, W. P.; de Gelder, R.; Israel, R.; Smits, J. M. M. *The DIRDIF-99 Program System*; Technical Report of the Crystallography Laboratory; University of Nijmegen: Nijmegen, The Netherlands, 1999.

(31) *Crystal Structure Analysis Package*; Rigaku and Rigaku/MSC, The Woodlands, TX, 2000−2006.

(32) Frisch, M. J.; Trucks, G. W.; Schlegel, H. B.; Scuseria, G. E.; Robb, M. A.; Cheeseman, J. R.; Montgomery, J. A., Jr.; Vreven, T.; Kudin, K. N.; Burant, J. C.; Millam, J. M.; Iyengar, S. S.; Tomasi, J.; Barone, V.; Mennucci, B.; Cossi, M.; Scalmani, G.; Rega, N.; Petersson, G. A.; Nakatsuji, H.; Hada, M.; Ehara, M.; Toyota, K.; Fukuda, R.; Hasegawa, J.; Ishida, M.; Nakajima, T.; Honda, Y.; Kitao, O.; Nakai, H.; Klene, M.; Li, X.; Knox, J. E.; Hratchian, H. P.; Cross, J. B.; Bakken, V.; Adamo, C.; Jaramillo, J.; Gomperts, R.; Stratmann, R. E.; Yazyev, O.; Austin, A. J.; Cammi, R.; Pomelli, C.; Ochterski, J. W.; Ayala, P. Y.; Morokuma, K.; Voth, G. A.; Salvador, P.; Dannenberg, J. J.; Zakrzewski, V. G.; Dapprich, S.; Daniels, A. D.; Strain, M. C.; Farkas, O.; Malick, D. K.; Rabuck, A. D.; Raghavachari, K.; Foresman, J. B.; Ortiz, J. V.; Cui, Q.; Baboul, A. G.; Clifford, S.; Cioslowski, J.; Stefanov, B. B.; Liu, G.; Liashenko, A.; Piskorz, P.; Komaromi, I.; Martin, R. L.; Fox, D. J.; Keith, T.; Al-Laham, M. A.; Peng, C. Y.; Nanayakkara, A.; Challacombe, M.; Gill, P. M. W.; Johnson, B.; Chen, W.; Wong, M. W.; Gonzalez, C.; Pople, J. A. *Gaussian 03*; Gaussian, Inc.: Pittsburgh, PA, 2003.

(33) Molecular orbitals were analyzed using the AOMix program [a, b]. (a) Gorelsky, S. I.; , AOMix: *Program for Molecular Orbital Analysis*; York University: Toronto, 1997; http://www.sh-chem.net/. (b) Gorelsky, S. I.; Lever, A. B. P. *J. Organomet. Chem.* **2001**, *635*, 187–196.

(34) O'Boyle, N. M.; Tenderholt, A. L.; Langner, K. M. *J. Comp. Chem.* **2008**, *29*, 839–845.

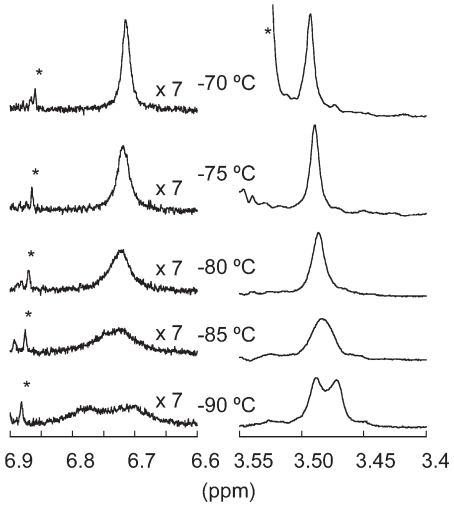

Figure 2. VT ^{1}H NMR spectra of **4** in $(CD_3)_2CO$. Asterisks indicate water or impurity.

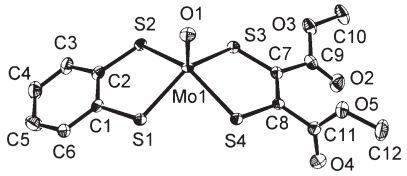

Figure 3. Crystal structure of the anionic part of $(Et_4N)(Ph_4P)$-$[MoO(S_2C_2(CO_2Me)_2)(bdt)]$ (**1a**) shown with 50% ellipsoids. The hydrogen atoms were omitted for clarity.

assigned to the $bdtCl_2^{2-}$ and $S_2C_2(CO_2CH_3)_2^{2-}$ protons, respectively. These signals broadened as the temperature of the solution was decreased to −85 °C, and each singlet was observed to split into two singlets at −90 °C. Upon cycling the temperature back to 25 °C, the original ^{1}H NMR spectrum was regenerated. The spectral changes observed for **4** were independent of concentration. These results indicate that **4** exhibits a structural isomerization between Δ and Λ forms (50%:50%). Compounds **2** and **6** also exhibit an isomerization behavior similar to that observed for **4**. The equation $\Delta G^{\ddagger} = RT_c = 22.96 + \ln(T_c/\delta v)$ was used to calculate $\Delta G^{\ddagger}$ for the isomerization process, and these values are found to be 40, 39, and 42 k J mol^{-1}, for **2**, **4**, and **6**, respectively.[35]

Crystal Structures of $Mo^{IV}O$ and $Mo^{VI}O_2$ Complexes. Although the synthesis of **1** was reported previously,[14] the crystal structure of the $(Et_4N)(Ph_4P)$ salt (**1a**) was determined in this work. The complex anion is shown in Figure 3 and the selected bond distances and angles are listed in Table 2. The Mo1 atom possesses a distorted square pyramidal geometry, with a terminal oxo, two sulfur atoms of bdt^{2-}, and two additional sulfur atoms of $S_2C_2(CO_2Me)_2^{2-}$, similar to that found in other structurally characterized bis(dithiolene)$Mo^{IV}O$ complexes including $(Et_4N)_2[Mo^{IV}O(S_2C_2(CO_2Me)_2)_2]$ (**5**) and $(Et_4N)_2[Mo^{IV}O(bdt)_2]$.[11−13,28,36]

(35) T_c and δ_v are the coalescence point and the frequency difference between sites in the exchange system, respectively. (Abraham, R. J.; Fisher, J.; Loftus, P. *Introduction to NMR Spectroscopy*; John Wiley and Sons Ltd.: Chichester, U.K., 1988.) T_c = 193, 188, 203 K and δ_v = 25.3, 29.6, and 28.1 Hz for 2, 4, and 6, respectively, were employed.

(36) Boyde, S; Ellis, S. R.; Garner, C. D.; Clegg, W. *J. Chem. Soc., Chem. Commun.* **1986**, 1541–1543.

Table 2. Selected Bond Distances (Å) and Angles (deg) of **1a**

Mo(1)−O(1)	1.696(2)	Mo(1)−S(1)	2.3785(8)
Mo(1)−S(2)	2.3905(8)	Mo(1)−S(3)	2.3863(8)
Mo(1)−S(4)	2.3988(8)	S(1)−C(1)	1.776(3)
S(2)−C(2)	1.774(3)	S(3)−C(7)	1.774(3)
S(4)−C(8)	1.753(3)	C(1)−C(2)	1.386(4)
C(7)−C(8)	1.356(4)	Mo(1)−4S plane	0.75
O(1)−Mo(1)−S(1)	108.75(8)	O(1)−Mo(1)−S(2)	107.05(8)
O(1)−Mo(1)−S(3)	109.98(8)	O(1)−Mo(1)−S(4)	107.24(8)
S(1)−Mo(1)−S(3)	141.26(2)	S(2)−Mo(1)−S(4)	145.70(2)
S(1)Mo(1)S(2)−S(1)C(1)C(2)S(2)[a]	8.097	S(3)Mo(1)S(4)−S(3)C(7)C(8)S(4)[a]	12.647

[a] Dihedral angle.

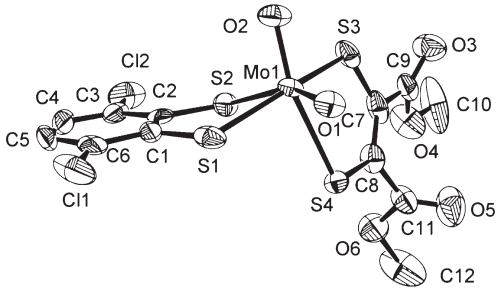

Figure 4. Crystal structure of the anionic part of $(Et_4N)(Ph_4P)[MoO(S_2C_2(CO_2Me)_2)(bdtCl_2)]$ (**4**) shown with 50% ellipsoids. The hydrogen atoms were omitted for clarity.

The crystal structure of the anionic part in **4** is shown in Figure 4, and the selected bond distances and angles are listed in Table 3. The Mo1 atom of **4** is coordinated by two oxo oxygen atoms (O1 and O2), two sulfur atoms (S1 and S2) from $bdtCl_2^{2-}$, and two sulfur atoms (S3 and S4) from $S_2C_2(CO_2Me)_2^{2-}$. The S2−S1−S3−S4 torsion angle describing the twist of the two dithiolene ligands relative to one another is 94.1°, indicative of a distorted octahedral geometry about the Mo1 center.[37] Similar to the crystal structures of $(Ph_4P)_2[Mo^{VI}O_2(bdt)_2]$,[27] $(Ph_4P)_2[Mo^{VI}O_2(mnt)_2]$,[19,27] and $(Et_4N)_2[Mo^{VI}O_2(bdtCl_2)_2]$,[23] the Mo1−S2 and Mo1−S4 bond distances (2.5537(19) and 2.6555(16) Å) are longer than the Mo1−S1 and Mo1−S3 distances (2.431(2) and 2.4059(18) Å) because S2 and S4 are oriented trans to the O1 and O2 oxo atoms. The structure of the $bdtCl_2^{2-}$ ligand in **4** is very similar to those observed in $(Et_4N)_2[Mo^{VI}O_2(bdtCl_2)_2]$,[23] reflecting π-delocalization with the aromatic ring. Interestingly, the S3−C7 (1.731(9) Å) and S4−C8 (1.720(7) Å) bond distances for the $S_2C_2(CO_2Me)_2^{2-}$ ligand are remarkably similar and do not reflect whether the S−C bonds are oriented trans or cis relative to the O2 oxo atom. The two S−C bond distances are significantly shorter than those observed in the $Mo^{IV}O$ complex, **1** (1.77 Å (average)). Large dihedral angles (30.3° and 75.7° for S3C7C8S3−O3C7O4 and S3C7C8S3−O5C11O6, respectively) are observed between the S3C7C8S3 and CO_2Me planes in **4**. This is indicative of a reduced conjugation between the ene-1,2-ditiolate and the CO_2Me substituents.

Two independent complexes (molecules a and b) are found in the unit cell of **6**. Crystal structures of **6a** and **6b** are depicted in Figures 5 and S4, Supporting Information, respectively. The two complex anions are different in the

(37) Webster, C. E.; Hall, M. B. *J. Am. Chem. Soc.* **2001**, *123*, 5820–5821.

Table 3. Selected Bond Distances (Å) and Angles (deg) of **4**, **6**, and **7**

	4	6a	6b	7
Mo(1)−O(1)	1.736(4)	1.725(3)	1.724(3)	1.732(3)
Mo(1)−O(2)	1.716(5)	1.719(3)	1.748(3)	1.739(3)
Mo(1)−S(1)	2.431(2)	2.4400(14)	2.4126(14)	2.4408(12)
Mo(1)−S(2)	2.5537(19)	2.6522(12)	2.6255(15)	2.6260(13)
Mo(1)−S(3)	2.4059(18)	2.4335(13)	2.4400(14)	2.4234(11)
Mo(1)−S(4)	2.6555(16)	2.6099(15)	2.5712(13)	2.6234(11)
S(1)−C(1)	1.747(10)	1.776(4)	1.747(4)	1.759(5)
S(2)−C(2)	1.740(9)	1.715(5)	1.714(5)	1.709(4)
S(3)−C(7)	1.731(9)	1.756(4)	1.728(4)	1.758(5)
S(4)−C(8)	1.720(7)	1.720(4)	1.742(5)	1.731(5)
C(1)−C(2)	1.394(11)	1.357(6)	1.377(7)	1.370(6)
C(7)−C(8)	1.355(11)	1.361(7)	1.359(6)	1.342(5)
O(1)−Mo(1)−O(2)	103.6(2)	104.48(17)	103.10(16)	102.93(16)
O(1)−Mo(1)−S(1)	82.78(19)	85.01(12)	82.74(11)	83.79(12)
O(1)−Mo(1)−S(3)	113.46(18)	105.79(11)	108.84(12)	109.05(13)
S(1)−Mo(1)−S(3)	161.13(8)	160.49(4)	160.18(4)	158.10(4)
S(2)S(1)S(3)S(4)[a]	94.1	95.1	99.7	99.4
S−C=C−S−OCO[b]	30.3, 75.7	20.2, 62.8	4.09, 89.5	5.71, 79.0
		20.4, 68.8	77.4, 18.8	2.4, 88.0
S(1)Mo(1)S(2)−S(1)C(1)C(2)S(2)[b]	21.5	5.5	6.4	6.4
S(3)Mo(1)S(4)−S(3)C(7)C(8)S(4)[b]	4.16	14.9	5.1	12.5

[a] Torsion angle. [b] Dihedral angle

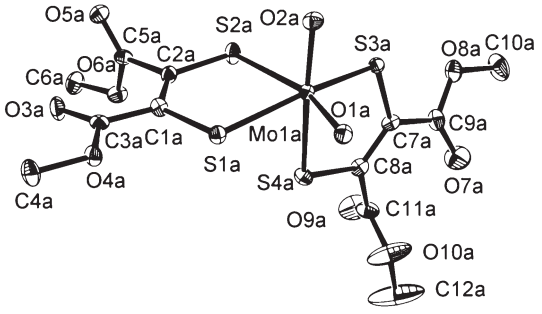

Figure 5. Crystal structure of one of the two independent anionic parts of $(Et_4N)(Ph_4P)[MoO_2(S_2C_2(CO_2Me)_2)_2]$ (**6**) (molecule **6a**) shown with 50% ellipsoids. The hydrogen atoms were omitted for clarity.

orientation of their $-CO_2Me$ groups with respect to the S−C−C−S plane (see Table 3). The stereochemistry about Mo1a is described as a distorted octahedron, and this is reflected by a S2aS1aS3aS4a dihedral angle (95.1°) close to 90°. The S2a−C2a (1.715(5) Å) and S4a−C8a (1.720(4) Å) bonds oriented trans to O1a and O2a are short because of the trans influence of the oxo groups. By comparison, the S−C bonds oriented cis to O1a and O2a are 1.776(4) Å and 1.756(4) Å, respectively. Interestingly, the S2a−C4a and S4a−C8a bond distances are shorter than the four S−C bonds (average distance, 1.76 Å) of the corresponding $Mo^{IV}O$ complex, **5**, and C1a−C2a and C7a−C8a (1.357(6) and 1.359(7) Å) bond distances are longer than the two C=C bonds (1.31(1) and 1.33 Å) of **5**.[28] Although a comparisons of these dimensions in **5** and **6** is suspect due to the calculated standard deviations, the observed ν(C=C) Raman stretching frequencies for the $S_2(C_2CO_2Me)_2$ units of **5** (1535 cm^{-1})[38] and **6** (1510 and 1494 cm^{-1}, vide infra) support this comparison. On the contrary, the dimensions of the $S_2(C_2CO_2Me)_2^{2-}$ ligands in molecule **6a** are similar to those observed in $(Ph_4P)_2[Mo^{IV}(S_2C_2(CO_2Me)_2)_3]$. The average S−C and C−C bond distances in $(Ph_4P)_2[Mo^{IV}(S_2C_2(CO_2Me)_2)_3]$ are 1.74 and 1.35 Å, respectively, indicative of a large π−delocalization between the Mo and $S_2(C_2CO_2Me)_2^{2-}$ units.[37] Collectively, the structural results indicate that $S_2C_2(CO_2Me)_2^{2-}$ of **6a** possesses a greater contribution of the dithione form than is observed for bdt^{2-} or $bdtCl_2^{2-}$.

The geometry about the molybdenum center (Mo1b) in **6b** is also best described as a distorted octahedron and possesses an S2bS1bS3bS4b torsion angle of ~100°. For one of the **6b** $S_2C_2(CO_2Me)_2^{2-}$ ligands, the S2b−C2b bond distance (1.714(5) Å) trans to O1b is noticeably shorter than the S1b−C1b bond distance (1.747(4) Å) cis to the oxo ligand, similar to what was observed for **6a**. The second $S_2C_2(CO_2Me)_2^{2-}$ ligand possesses a S4b−C8b bond distance (1.742(5) Å) trans to O2b, which is close to that observed in the cis position (1.728(4) Å), rather the former is slightly longer than the latter. These S−C bond distance differences are not as significant as those observed in **6a**. The four S−C bonds are shorter than those observed in **5**, while the two C=C bonds are longer. These comparisons suggest that the $S_2C_2(CO_2Me)_2^{2-}$ ligands of **6b** also possess some dithione character. Although both **6a** and **6b** possess $S_2C_2(CO_2Me)_2^{2-}$ ligands with some dithione character, the primary structural differences between **6a** and **6b** likely result from crystal packing forces. The metric parameters for $(Et_4N)_2[MoO_2(S_2C_2(CO_2Me)_2)]$ (**7**) are close to those observed in molecule **6a** but not **6b** as indicated by the shorter S2−C2 (1.709(4) Å) and S4−C8 (1.731(5) Å) as compared with S1−C1 (1.759(5) Å) and S3−C7 (1.758(5) Å) of **7**.

Spectroscopy and Electronic Structure. Despite the different ligand sets in **2**, **4**, and **6**, the solution electronic absorption spectra of the complexes are remarkably similar and display three bands below 30 000 cm^{-1} (Figure 6). The d^0 nature of the Mo(VI) ion and the magnitude of the extinction coefficients (~2000−8000 M^{-1} cm^{-1}) for these three bands clearly identify the

(38) Subramanian, P.; Burgmayer, S.; Richard, S.; Szalaki, V.; Spiro, T. G. *Inorg. Chem.* **1990**, *29*, 3849–3853.

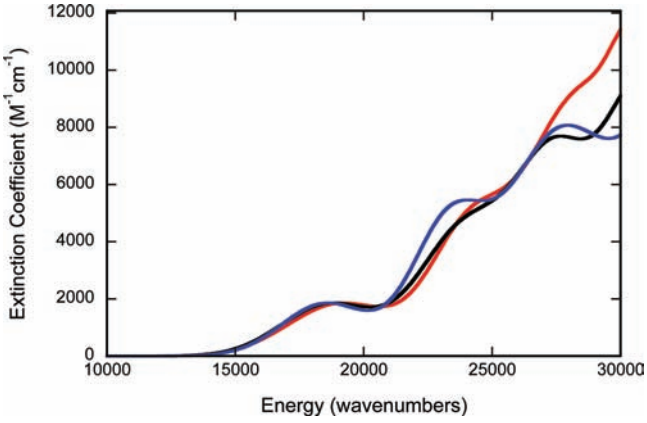

Figure 6. Solution electronic absorption spectra for **2** (black), **4** (red), and **6** (blue). Extinction coefficients have been normalized to the 18 000 cm^{-1} band for comparative purposes.

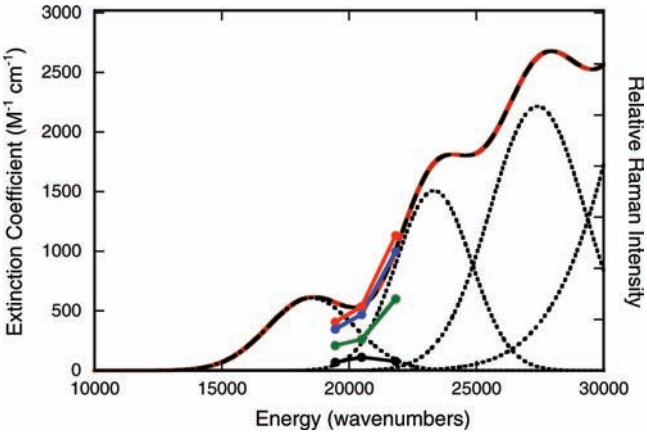

Figure 7. Gaussian resolved electronic absorption spectrum for **6**. Resonance Raman excitation profiles are shown for the 867 cm^{-1} symmetric $O_{oxo}-Mo-O_{oxo}$ stretch (red), 1494 cm^{-1} C=C stretch (green), 1510 cm^{-1} C=C stretch (blue), and 834 cm^{-1} asymmetric $O_{oxo}-Mo-O_{oxo}$ stretch (black).

transitions in this energy range as ligand-to-metal charge transfer (LMCT) in nature. Because of the spectral similarity between complexes **2**, **4**, and **6**, we will focus our discussion on compound **6**, whose Gaussian resolved solution electronic absorption spectrum is presented in Figure 7.

Although **2**, **4**, and **6** possess no molecular symmetry, the dominant dioxo ligand field principally dictates the nature of the Mo d orbitals. These vacant d molecular orbitals are the lowest energy acceptor orbitals and they are depicted in Figure 8 for compound **6**. The orbital plots are shown at an isodensity value of 0.05 au to more clearly depict the nature of the Mo d orbital component in these low-lying virtual molecular orbitals. The five lowest-energy acceptor orbitals (LUMO − LUMO+4) possess d orbital functions that are π antibonding with respect to the two oxo ligands. The LUMO and LUMO+1 are the lowest energy orbitals because of their weak π interactions with the oxo ligands. Their relative energy ordering is a function of the $O_{oxo}-Mo-O_{oxo}$ bond angle, with more acute angles leading to an orbital reversal between LUMO and LUMO+1. The LUMO+2, LUMO+3, and LUMO+4 orbitals possess Mo d orbital

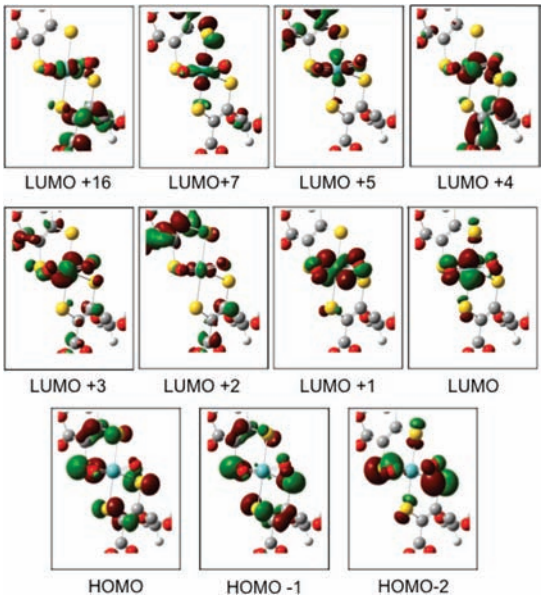

Figure 8. Calculated active space HOMO and LUMO wave functions for **6** depicted at an isodensity value of 0.05 au.

functions that are more strongly π-antibonding with respect to the oxo ligands due to the increased directionality of the π-bond along the $Mo-O_{oxo}$ bond axes, and this leads to their higher energy. Additionally, the LUMO+2, LUMO+3, and LUMO+4 orbitals possess dithiolene C=C antibonding character, which is not present to a large degree in the LUMO and LUMO+1. Thus, one-electron promotions to LUMO+2, LUMO+3, and LUMO+4 acceptor orbitals should result in larger excited state distortions along the C=C and symmetric $O_{oxo}-Mo-O_{oxo}$ stretching coordinates. The LUMO+5 and LUMO+7 are at higher energy because they are σ antibonding with respect to the two trans dithiolene sulfur donors. Therefore, LMCT transitions to LUMO+5 and LUMO+7 are not likely to be observed at energies less than ~25 000 cm^{-1}. The LUMO+16 orbital is found at very high energy since the Mo d orbital component of this LUMO is σ antibonding with respect to the two oxo ligands and the cis dithiolene sulfur donors.

The bonding calculations indicate that the two highest occupied molecular orbitals (HOMOs) of the bis-dithiolene ligand set comprise in-phase and out-of-phase combinations of out-of-plane symmetric dithiolene sulfur p orbitals (HOMO and HOMO−1 in Figure 8), and this is in agreement with earlier work on mono-oxomolybdenum dithiolene complexes.[8,39] The HOMO−2 function is at deeper binding energy and can be described as an out-of-phase linear combination of out-of-plane dithiolene sulfur p orbitals localized on the cis dithiolene sulfur atoms (Figure 8). Further inspection of the calculated orbital energies indicates that HOMO and HOMO−1 are relatively close in energy (ΔE = 3300 cm^{-1}), while LUMO and LUMO+1 are nearly isoenergetic (ΔE = 1800 cm^{-1}) (Figure 8). The near degeneracy of the LUMO and LUMO+1 orbitals in **2**, **4**, and **6** is markedly different from what is observed in the

(39) Inscore, F. E.; McNaughton, R.; Westcott, B. L.; Helton, M. E.; Jones, R.; Dhawan, I. K.; Enemark, J. H.; Kirk, M. L. *Inorg. Chem.* **1999**, *38*, 1401–1410.

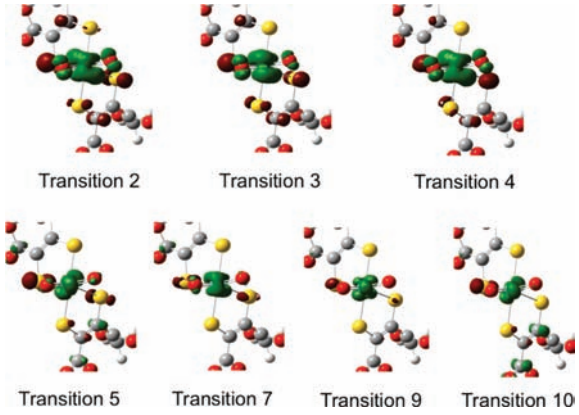

Figure 9. Calculated electron density difference maps (EDDMs) of transitions 2, 3, 4, 5, 7, 9, and 10 for **6** depicted at an isodensity value of 0.005 au. Transitions 2 and 3 are the dominant contributors to band 1, and transitions 4, 5, 7, 9, and 10 are the dominant contributors to band 2. Red regions indicate a loss of electron density in a transition to the excited state and green regions indicate a gain of electron density in a transition to the excited state.

5-coordinate dioxo active site of sulfite oxidase, where a large splitting between the LUMO and LUMO+1 is observed.[40,41] The relevant HOMO and LUMO orbitals for **2** and **4** are virtually identical to those of **6** and are provided in the Supporting Information (Figures S5 and S7).

Having described an active space of metal and ligand frontier orbital functions, we can now begin to describe the nature of the lowest-energy LMCT transitions in **2**, **4**, and **6**. Energy considerations indicate that the lowest-energy LMCT excitations should occur between the HOMO−1, HOMO, LUMO, and LUMO+1. Thus, there are four possible one-electron promotions that can occur between these orbitals and they should dominantly contribute to the lowest energy band. This is supported by the results of time-dependent DFT (TDDFT) calculations where it is found that two LMCT transitions (T2 and T3) arising from a linear combination of HOMO → LUMO+1 and HOMO−1 → LUMO one-electron promotions possess the highest oscillator strengths and dominate in their contribution to Band 1. The nature of the LUMO and LUMO+1 indicate that one-electron promotions to these acceptor orbitals will result in excited state distortions along the totally symmetric $O_{oxo}-Mo-O_{oxo}$ bend and weaker excited state distortions along the symmetric $O_{oxo}-Mo-O_{oxo}$ stretch. The mixing of these two one-electron promotions is clearly evident in the electron density difference maps (EDDMs) that are shown in Figure 9. Transitions 4, 5, 7, 9, and 10 are the LMCT transitions that principally contribute to the absorption envelope of band 2. The calculations indicate that HOMO−1 → LUMO+1 (T4) and HOMO → LUMO+3 (T5) one-electron promotions contribute to the low energy side of band 2. The dominant transition (T7) that contributes to band 2 is principally composed of HOMO−2 → LUMO and HOMO → LUMO+2 one-electron promotions. Additional LMCT transitions, assigned principally assigned as HOMO−1 → LUMO+3 (T9) and HOMO → LUMO+4 (T10) complete the high-energy envelope of band 2. The nature of the dominant LMCT transitions that comprise band 2 are summarized in the EDDMs shown in Figure 9. The electronic origin of band 3 is markedly more complex than that of bands 1 and 2 because of the large density of excited states expected in this spectral region. Calculations indicate that band 3 is comprised of numerous transitions of varying oscillator strength and that the HOMO−1→LUMO+5 one-electron promotion predominates in the transition that principally contributes to the intensity of this band.

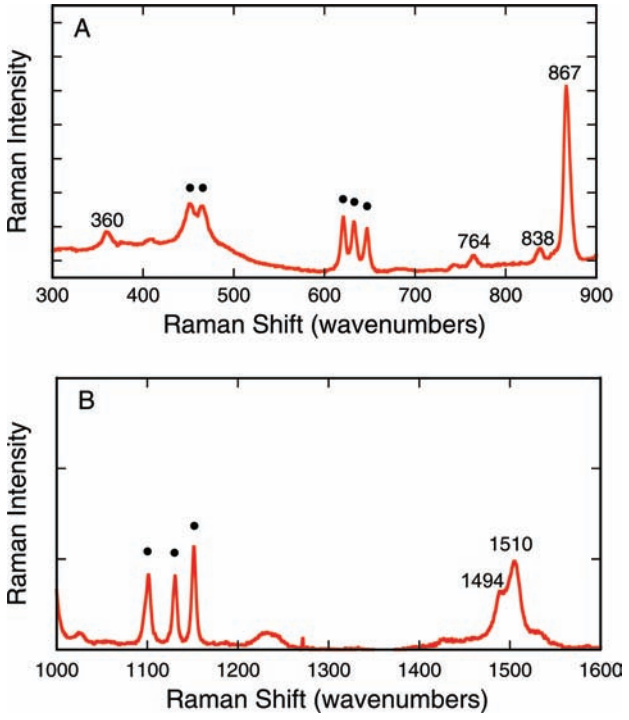

Figure 10. Low frequency (A) and high frequency (B) resonance Raman spectra of **6** using 458 nm excitation. Raman bands for the Na_2SO_4 internal standard are indicated with black dots. Vibrational assignments are given in Table 4.

The resonance Raman spectrum of **6** using 458 nm excitation is presented in Figure 10. We have observed $Mo-(S_{dt})_4$ and $O_{oxo}-Mo-O_{oxo}$ metal−ligand stretching modes as well as ligand based ene-1,2-dithiolate C−S and C=C stretches, and their corresponding vibrational frequencies are listed in Table 4. The frequency assignments have been assisted by direct spectral comparison with previously published Raman data for various DMSO reductase family enzymes as well as data for relevant $[Mo^{VI}O_2(dithiolene)_2]^{2-}$ model complexes.[7] In general, the experimental vibrational frequencies for **2**, **4**, and **6** are in reasonable agreement with the DFT calculated frequencies for these modes (Table 4). Resonance Raman excitation profiles have been constructed for the dithiolene C=C stretches and the symmetric and antisymmetric $O_{oxo}-Mo-O_{oxo}$ stretches in compound **6**. The excitation profiles are shown superimposed on the Gaussian resolved electronic absorption spectrum in Figure 7. Collectively, the resonance Raman enhancement profiles provide strong support for our LMCT assignments and the nature of the lowest-lying Mo-based acceptor orbitals. Specifically, the observed larger resonance

(40) Peariso, K.; McNaughton, R. L.; Kirk, M. L. *J. Am. Chem. Soc.* **2002**, *124*, 9006–9007.
(41) Hemann, C.; Hood, B. L.; Fulton, M.; Hansch, R.; Schwarz, G.; Mendel, R. R.; Kirk, M. L.; Hille, R. *J. Am. Chem. Soc.* **2005**, *127*, 16567–16577.

Table 4. Summary of Resonance Raman Data for Compounds **2**, **4**, and **6**

compound **2**		
vibrational mode	frequency (cm^{-1}) (observed)	frequency (cm^{-1}) (calculated)
Mo−$(S_{dt})_4$ (sym)	360	352
O_{oxo}−Mo−O_{oxo} (sym)	870	946
O_{oxo}−Mo−O_{oxo} (anti)	834	906
C−S stretch	764	764
C=C stretch	1497	1512
compound **4**		
vibrational mode	frequency (cm^{-1}) (observed)	frequency (cm^{-1}) (calculated)
Mo−$(S_{dt})_4$ (sym)	360	352
O_{oxo}−Mo−O_{oxo} (sym)	871	949
O_{oxo}−Mo−O_{oxo} (anti)	838	909
C−S stretch	765	765
C=C stretch[a]	1497	1516
compound **6**		
vibrational mode	frequency (cm^{-1}) (observed)	frequency (cm^{-1}) (calculated)
Mo−$(S_{dt})_4$ (sym)	360	353
O_{oxo}−Mo−O_{oxo} (sym)	867	944
O_{oxo}−Mo−O_{oxo} (anti)	838	922
C−S stretch	764	765
C=C stretch[a]	1494/1510	1510/1538

[a] Note: there are two distinct molecules of **6** in the unit cell.

enhancement of the symmetric O_{oxo}−Mo−O_{oxo} stretch upon excitation into the low energy side of Band 2 is fully consistent with the population of acceptor orbitals (LUMO+2, +3, +4) being strongly π-antibonding with respect to both oxo ligands. The resonance Raman excitation profiles for the two ene-1,2-dithiolate C=C stretches in **6** indicate that both of the ene-1,2-dithiolates are involved in LMCT transitions to the Mo center.

Bands 1−3 result from $S_{dithiolene} \rightarrow$ Mo charge transfer transitions, and their intensities are a direct reflection of the degree of $S_{dithiolene} \rightarrow$ Mo charge donation present in $[MoO_2(dithiolene)_2]^{2-}$ complexes. It is this charge donation that reflects Mo(VI) contributions to the Mo(VI/V) redox couple by reducing the hard donor stabilization of the Mo(VI) oxidation state and facilitating reductive processes at the metal. Oxygen atom transfer from $[MoO_2]^{2+}$ centers to oxygen atom acceptors represents a two-electron reductive process at the Mo site, and it has been observed that a linear correlation exists between $E_{1/2}$ and the rate of oxygen atom transfer to PPh_3.[42] The implication here is that the activation energy for oxygen atom transfer possesses a considerable contribution from partial electron occupancy of the Mo(VI) LUMO

(42) (a) Topich, J.; Lyon, J. T. *Inorg. Chem.* **1984**, *23*, 3202–3206. (b) Hammes, B. S.; Chohan, B. S.; Hoffman, J. T.; Einwachter, S.; Carrano, C. J. *Inorg. Chem.* **2004**, *43*, 7800–7806. (c) Basu, P.; Nemykin, V. N.; Senger, R. S. *Inorg. Chem.* **2009**, *48*, 6303–6313.

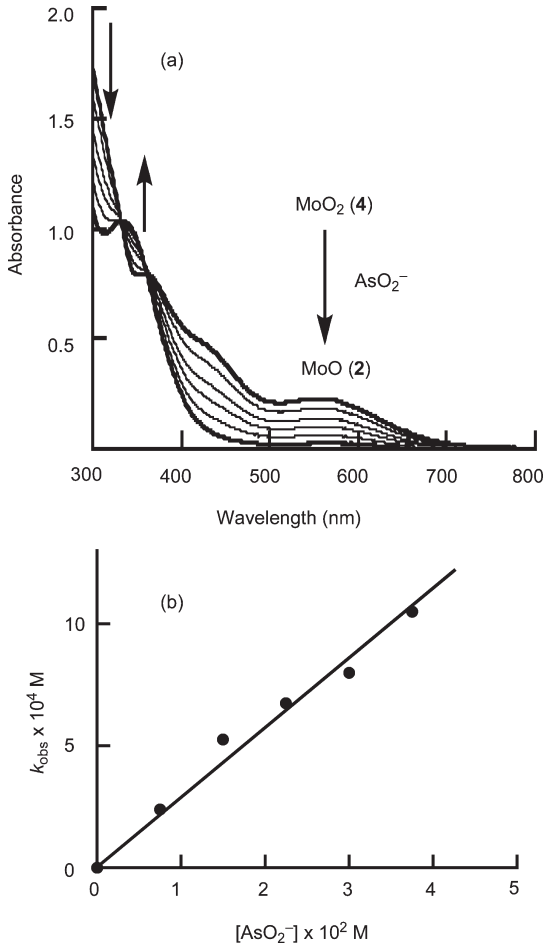

Figure 11. (a) Spectral change of **4** (1.5×10^{-4} M) reacted with $NaAsO_2$ (7.5×10^{-3} M) in CH_3CN-H_2O (3:2) at 20 °C, recorded every 60 s. (b) Pseudo-first-order rate constants k_{obs} as a function of [$NaAsO_2$].

at the transition state. Therefore, Mo-dithiolene covalency can modulate the reduction potential of $[MoO_2]^{2+}$ complexes by reducing the hard donor stabilization of the Mo(VI) state, leading to an increase in the rate of oxygen atom transfer to oxygen atom acceptors. Addtionally, electron occupation of the LUMO along the reaction coordinate will assist in the cleavage of the Mo=O bond in oxygen atom transfer reactions with oxo acceptors because of the O=Mo=O π*-character of the LUMO. Since both the low-energy LUMO and LUMO+1 are weakly O=Mo=O π-antibonding in these pseudo C_2 symmetry dioxo complexes, electron occupation of the LUMO and LUMO+1 will not make a substantial contribution to lowering the activation energy for oxygen atom transfer to yield a Mo(IV) mono-oxo complex. This is in marked contrast to the situation proposed for the five coordinate active site found in sulfite oxidizing enzymes, where the LUMO is *strongly* π-antibonding with respect to a single oxo ligand.[40,41] The similar LMCT spectra for **2**, **4**, and **6** imply very similar ligand field splitting patterns and similar degrees of Mo-dithiolene covalency. In the next section, we use the nature of the LMCT transitions and the corresponding electronic structures for these $[MoO_2(dithiolene)]^{2-}$ complexes to gain insight into their relative oxygen atom transfer rates.

Oxygen Atom Transfer Reactivity of $Mo^{VI}O_2$ Complexes. We investigated oxygen atom transfer reactions from

the $Mo^{VI}O_2$ complexes, **2**, **4**, and **6**, to AsO_2^-, which is a native substrate of the DMSOR family enzyme arsenite oxidase.[9] Compounds **4** and **6** transferred a single oxygen atom to AsO_2^- to yield the corresponding $Mo^{IV}O$ species, **3** and **5**, and AsO_3^- stoichiometrically. In contrast, **2** dispropotionated into 0.5 equiv of $[Mo^{VI}O_2(bdt)_2]^{2-}$ and 0.5 equiv of **6** to eventually yield the corresponding $Mo^{IV}O$ species after a prolonged reaction time. As a result, we determined the rates of reaction for **4** and **6** with AsO_2^- spectroscopically. The time course of reaction for **4** is illustrated in Figure 11a. Here, the characteristic bands at 418 and 525 nm were observed to decrease in intensity with time, obeying pseudo-first-order kinetics. The observed rate constant (k_{obs}, s^{-1}) was proportional to the AsO_2^- concentration, and saturation kinetics was not observed even at high AsO_2^- concentration (Figure 11b). Thus, this oxygen atom transfer was analyzed as a second-order reaction, $v = k[MoO_2][AsO_2]$, and the rate constant k was calculated to be 2.7×10^{-2} M^{-1} s^{-1}. Oxygen atom transfer from **6** to AsO_2^- was also analyzed as a second order reaction and its rate constant k was determined to be 2.7×10^{-2} M^{-1} s^{-1}. In molybdenum complexes that show a reversible Mo(VI)/Mo(V) redox process, the reduction potential provides a good indication of their relative oxygen atom transfer reaction rates.[43−45] Although irreversible redox behavior is observed for **4** and **6**, the small difference in their redox potential values support their identical reaction rates. This result is consistent with the observation of similar LMCT spectra for these complexes as well as similar Mo═O bond strengths inferred from their $O_{oxo}-Mo-O_{oxo}$ stretching frequencies (873 cm^{-1} for **4** and 869 cm^{-1} for **6**).

(43) Izumi, Y.; Glaser, T.; Rose, K.; McMaster, J.; Basu, P.; Enemark, J. H.; Hedman, B.; Hodgson, K. O.; Solomon, E. I. *J. Am. Chem. Soc.* **1999**, *121*, 10035–10046.
(44) Sung, K.-M.; Holm, R. H. *J. Am. Chem. Soc.* **2002**, *124*, 4312–4320.
(45) Kail, B. W.; Perez, L. M.; Zaric, S. D.; Milar, A. J.; Young, C. G.; Hall, M. B.; Basu, P. *Chem.—Eur. J.* **2006**, *12*, 7501–7509.

Conclusions

We have shown that $Mo^{VI}O_2$ complexes with either one aliphatic ene-1,2-dithiolate ligand ($S_2C_2(CO_2Me)_2^{2-}$) (**2** and **4**) or two aliphatic ene-1,2-dithiolate ligands (**6**) are isolable. This has enabled their structures to be determined by X-ray crystallography, as well as detailed investigations of their solution structure, oxygen atom transfer reactivity, and electronic structure by variable-temperature ^1H NMR, electronic absorption, and resonance Raman spectroscopies. The crystallographic, computational, and spectroscopic results indicate the presence of considerable π-delocalization between the $Mo^{VI}O_2$ and ($S_2(C_2(CO_2Me)_2^{2-}$) units. This is interpreted to result in a greater $Mo^{VI}-S$ bond covalency in **2**, **4**, and **6** as compared with $[Mo^{IV}O(S_2(C_2(CO_2Me)_2)_2]^{2-}$. Solution electronic absorption spectra and resonance Raman excitation profiles have allowed for the assignment of the lowest energy LMCT transitions in **2**, **4**, and **6**. Variable-temperature NMR spectra of the $Mo^{VI}O_2$ complexes indicated an isomerization between Δ and Λ forms of an octahedral structure in $(CD_3)_2CO$. Finally, the kinetic studies of the $Mo^{VI}O_2$ complexes have provided insight into the relationship between their electronic structure and oxygen atom transfer reactivity.

Acknowledgment. This work was partly supported by a grant for Scientific Research (No. 20550067 to H.S.) from the Japan Society for Promotion of Science. M.L.K. acknowledges the National Institutes of Health (GM-057378) for financial assistance.

Supporting Information Available: ESI−mass spectra of **2**, **4**, and **6** (Figures S1−S3), crystal structures of **6b** and **7** (Figures S4 and S5), CIF files of **1a**, **4**, **6**, and **7**, and relevant molecular orbitals for **2** and **4** (Figures S6 and S7). This material is available free of charge via the Internet at http://pubs.acs.org.